VPS VIBRATIONS IN PHYSICAL SYSTEMS

DOI: 10.21008/j.0860-6897.2023.1.09
Vibrations in Physical Systems, 2023, 34(1), 2023109

Noise effect on parameters of quiet sonar with code modulation

Roman SALAMON, Jacek MARSZAL, Andrzej JEDEL

Gdansk University of Technology, Faculty of Electronics, Telecommunications and Informatics, Department of Sonar Systems, ul. Narutowicza 11/12, 80-233 Gdańsk, Poland

Corresponding author: Jacek Marszal, email: jacek.marszal@pg.edu.pl

Abstract Earlier publications of the paper authors have shown that the use of code keying mixed with the CW FM sound signal allows the significant reduction in the distance measurement error, compared to classic silent CW FM sonar. In addition to the code modulation parameters, the magnitude of this error is influenced by the received input acoustic noise. The article shows the dependence of the input signal-to-noise ratio and the sound signal parameters on the target distance measurement error and the detection conditions, such as the output signal-to-noise ratio and the side lobe level. The results of the analysis were compared to the same parameters of the CW FM silent sonar without code modulation.

Keywords: silent sonar, maximum length sequence, signal-to-noise ratio, frequency modulation.

1. Introduction

A disadvantage of an active sonar system is the capacity to detect the sound signals emitted by receiving systems installed on foreign naval vessels. Detection may be hindered by reducing the power of the sound signals as well as by using the signals required by the matched filtration receiver. The amplitude of an echo signal at the output of the matched filtration system is proportional to its energy, which is equal to the product of its power and duration. To reduce signal power at a constant level of desired energy, signals with the longest possible duration should be used. A natural solution in this respect involves continuous-wave frequency-modulated (CWFM) sound signals. Linear frequency modulation (LFM) or hyperbolic frequency modulation (HFM) can also be used. In both cases, the reduction in the detection capacity by foreign listening systems is very efficient [1-4]. The main disadvantage of the CWFM systems is the significant error in target distance measurement caused by the movement of the sonar and/or the observed target. As a result of the associated Doppler effect, the distance measurement error increases with increases in signal speed and duration, and amounts to values difficult to accept in practice [5, 6].

Attempts have been taken to reduce the target distance measurement error by using frequency-modulated signal coding [4, 7, 8]. Maximum length sequence (MLS) code has been used, featuring a narrow correlation function with a low level of side lobes. This solution gives satisfactory results, but it is compromised with the deterioration in deep resolution. It is required to carry out a thorough analysis of the impact of acoustic noise on the detection conditions for sound signal coding. This is the subject matter of this article. The results of the analysis were compared to the results concerning the CWFM sonar without code modulation. Similar phenomena related to the Doppler effect also occur in underwater acoustic communication systems using signals with spread spectrum [9-11].

2. Operating principle of a sonar receiver with code modulation

A functional diagram of the sonar is shown in Fig. 1. To simplify, we assumed that the echo signal was a delayed periodic sequence of the sound signal modified by the Doppler effect. This sequence with a hyperbolic frequency modulation (HFM) was modulated by a maximum length sequence (MLS). An MLS of the desired order of M, comprising rectangular pulses of selected duration T_i and repeated every T, was selected, see Fig. 2. Each rectangular pulse was filled with a hyperbolic frequency modulation signal of bandwidth B. Signals in the positive and negative pulses had spectra shifted relative to each other (see Fig. 3) and additionally differed in terms of the direction of frequency variations. They were described using the following formulae:

$$s_l(t) = s_o \sin\left[-2\pi \frac{T_i f_l f_h}{B} ln\left(1 - \frac{B}{f_h T} dt\right)\right], \qquad s_h(t) = s_o \sin\left[2\pi \frac{T_i f_l f_h}{B} \ln\left(1 + \frac{B}{f_l T} dt\right)\right], \tag{1}$$

where: $s_l(t)$ was the low frequency band signal, $s_h(t)$ the high frequency band signal, f_l and f_h described the lower and upper frequencies of these signals, respectively, and $d = (c + v)/(c - v)$ was the coefficient of time compression for a target moving at speed v.

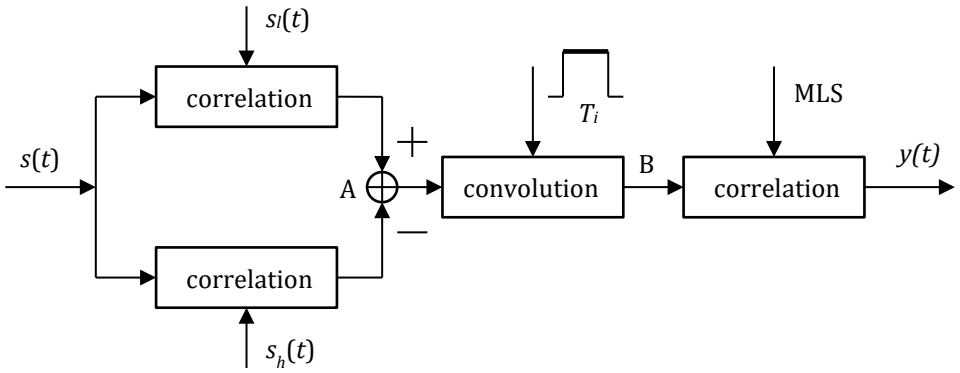

Figure 1. Functional diagram of signal processing in a sonar receiver.

An input signal was correlated with a low-band reference signal and with a high-band reference signal. The spectra of these signals are shown in black in Fig. 3. The signals were totalled after correlation and the introduction of a delay, see Fig. 4 for the output signal received. This was a narrow-band copy of a maximum length sequence of a signal without the Doppler effect. A delayed signal $s_h(t)$ was convoluted with a rectangular pulse of duration T_i. The resulting convolution is shown in Fig. 5. It was an analogue equivalent to the maximum length sequence.

Attention should be paid to the inverse direction of shifting impulses with the Doppler effect for positive and negative pulses. This was able to reduce the target distance measurement error.

The last operation consisted in determining the correlation between the signal $x_h(t)$ and the reference signal $x(t)$, presented in black in Fig. 2. To avoid transients, the signal $x_h(t)$ must be periodic. For clarification, only two MLS cycles are presented in Fig. 6.

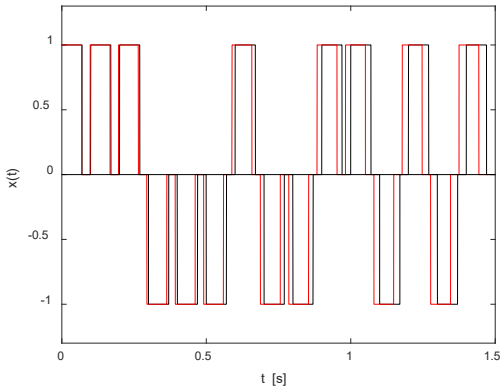

Figure 2. One cycle of MLS rectangular pulse (black line - without the Doppler effect, red line - with the Doppler effect, $M = 4$, $T = 0.1$ s, $T_i = 0.07$ s, $v = 13.5$ m/s).

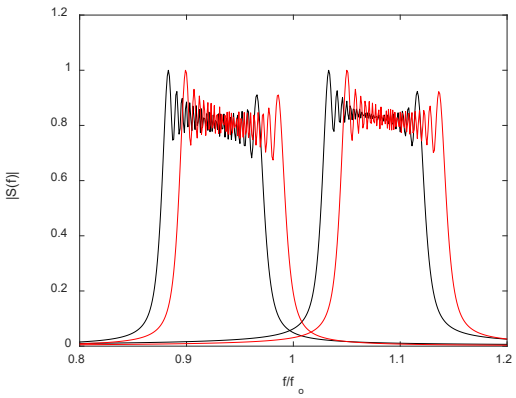

Figure 3. HFM signal spectra (black line - without the Doppler effect, red line - with the Doppler effect, $f_0 = 10$ kHz, low band $f_l = 8.75$ Hz, $f_h = 9.75$ Hz, high band $f_l = 10.25$ Hz, $f_h = 11.25$ Hz, $v = 13.5$ m/s).

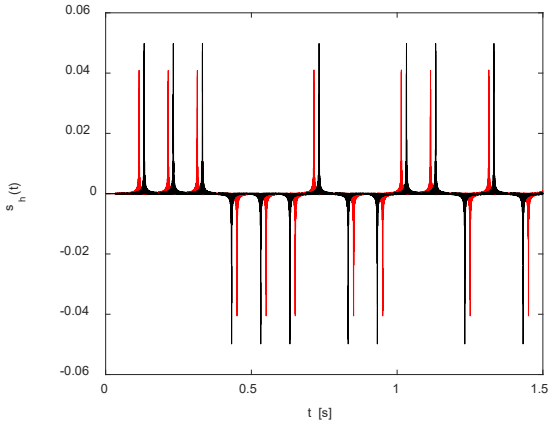

Figure 4. Signal at the adder output (point A on Fig. 1). Black line - without the Doppler effect, red line - with the Doppler effect.

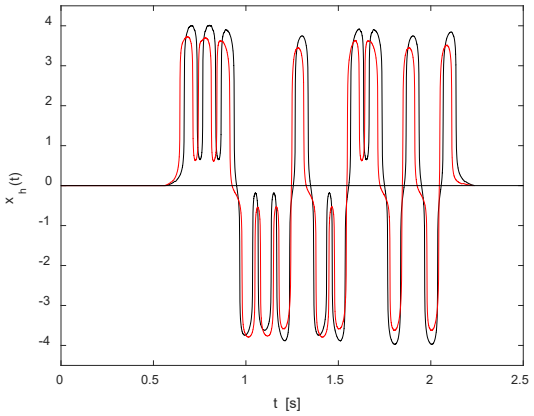

Figure 5. Signal after convolution (point B on Fig. 1). Black line - without the Doppler effect, red line - with the Doppler effect.

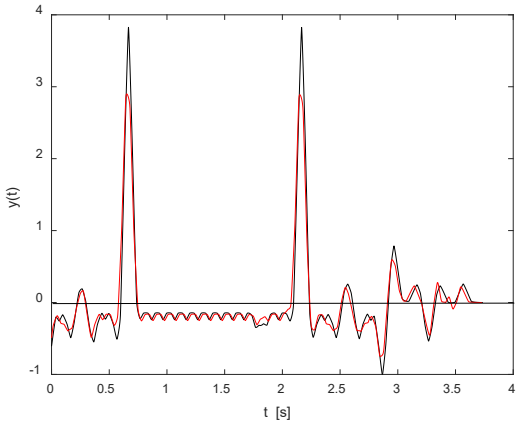

Figure 6. Output signal. Black line - without the Doppler effect, red line - with the Doppler effect.

3. Impact of system operations on noise

Every operation related to the echo signal as described in the preceding section improved the output signal-to-noise ratio. Therefore, a received signal $s(t)$ with hyperbolic frequency modulation was correlated with a noiseless reference signal $w(t)=[s_l(t), s_h(t)]$. Fig. 7 shows an autocorrelation function $r_{ww}(t)$ of the reference signal, while Fig. 8 shows the correlation function $r_{sw}(t)$ of a signal $s(t)$ being the sum of the signal $w(t)$ and white Gaussian noise $n(t)$.

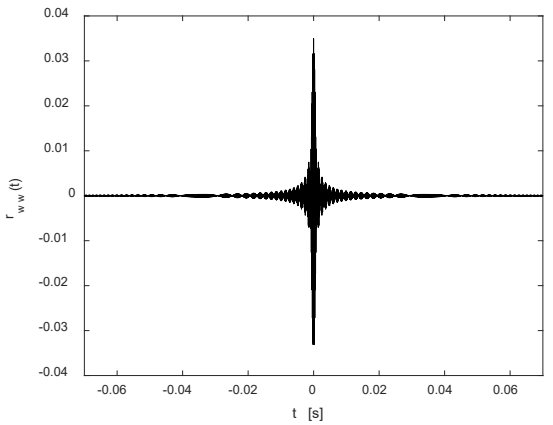

Figure 7. Autocorrelation function of HFM reference signal (f_l = 8.75 Hz, f_h = 9.75 Hz, T = 0.1 s, T_i = 0.07 s, s_o = 1, σ = 0).

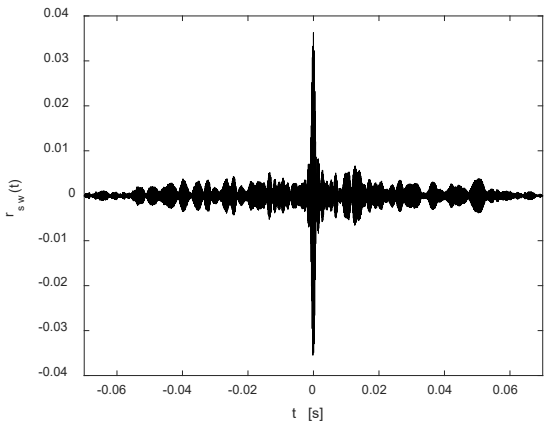

Figure 8. Function of correlation of HFM signal with noise with HFM reference signal. (parameters as in Fig. 7, σ = 3).

From here on, the input signal-to-noise ratio expressed in decibels should be defined as follows:

$$SNR_i = 10 \log_{10} \frac{P_i}{P_n}, \tag{2}$$

with P_i as signal power at the system input and P_n as noise power at the system input within its frequency bandwidth.

In the example provided in the figures above, P_i = 0.5 W, P_n = 0.36 W, thus SNR_i = 1.4 dB. The output signal-to-noise ratio was calculated according to the following formula:

$$SNR_{\text{out}} = 10 \log_{10} \frac{A^2}{P_{no}}, \tag{3}$$

where: A was the maximum value of the output signal and P_{no} the noise power.

In the example, A = 0.035 W and P_{no} = $65 \cdot 10^{-6}$ W. Therefore the output signal-to-noise ratio was equal to: SNR_{out} = 22.7 dB. As a consequence there was an increase in the signal-to-noise ratio: $dSNR$ = SNR_{out} - SNR_i = 21.3 dB. According to the theory [12], this increase amounted to $dSNR = 10 \log_{10} (2BT_i)$. For B = 1 kHz and T_i = 0.07 s assumed in the example, the increase is $dSNR$ = 21.4 dB, where 0.1 dB was the numerical simulation accuracy.

Switching to noise in the MLS signal, the impact of noise on a numerical sequence of MLS was shown first. Figure 9 shows three MLS cycles described as $x(n)$, containing M = 15 elements and a sum of these MLS cycles and noise with standard deviation σ. The correlation function $r_{xn}(n)$ was calculated by correlating $x(n)$ + noise (n) with a single MLS cycle. The result of the calculations is given in Fig. 10.

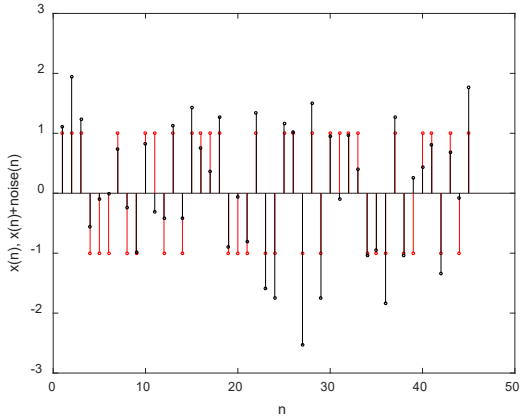

Figure 9. Three MLS cycles (red) and three MLS cycles with noise (black). (M = 15, σ = 0.7).

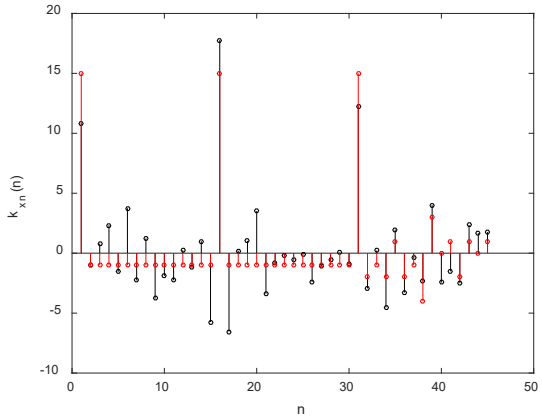

Figure 10. Autocorrelation function of MLS (red) and correlation function of MLS (black) with noise and one MLS cycle.

For the MLS parameters provided in the captions to Fig. 9 from formula (2), an input signal-to-noise ratio was determined: SNR_i = 3.1 dB. The output SNR_{out} was calculated according to (3) by entering A = 15 and P_{no} = 14.1. The result was SNR_{out} = 12.0 dB. It should be noted that noise has a constant component with a mean value of 1, equal to the value of the side lobes of the autocorrelation function for MLS (red chart in Fig. 10). The improvement in the signal-to-noise ratio was $dSNR$ = 8.9 dB. If noise power P_{no} was replaced in the formula (3) with a noise variance σ^2 = 7.8 (thus omitting its mean value), the output signal-to-noise ratio SNR_{out} = 14.6 dB and the improvement in the signal-to-noise ratio $dSNR$ = 11.5 dB were obtained. It was almost equal to $10 \log_{10} M$ = 11.7 dB. A small difference of 0.2 dB should be assigned to the noise variance numerical calculation error.

In summing up, it could be claimed (as confirmed by the calculations) that the improvement in the signal-to-noise ratio resulting from the correlation of MLS's was equal to $dSNR = 10 \log_{10} M$ for sequences with a variable number of elements M.

The last operation carried out in the system was the correlation of analogue MLS's designated as $x(t)$. Figure 11 shows MLS cycles, with and without noise. The following figures provided correlation functions $r_{xn}(t)$ of three MLS cycles with and without noise. Three sequences with noise and one sequence without noise were correlated. The figures illustrated the impact of the method of observation of the correlation function: full correlation function, its absolute value, and its positive path.

Depending on the method of observation and the assumed definition of the output signal-to-noise ratio, different values of this ratio could be obtained. Therefore, for the parameters given in captions to the figures, the output signal ratios were as follows when P_{no} in the formula (3) was determined using:

- noise power SNR_p = 21.8 dB,
- noise variance SNR_v = 23.5 dB,
- power of positive noise values SNR_0 = 31.6 dB.

The theoretical value of the output signal-to-noise ratio of the correlation receiving system was described using the following value [12]:

$$SNR_{out} = 10 \log_{10} \frac{A^2}{P_{no}}, \tag{4}$$

where E was signal energy and N was noise spectral power density.

In the example under consideration SNR_t = 23.3 dB and was almost equal to SNR_0 measured using noise variance (as for the numerical MLS).

To determine the output signal ratio, it was required to know the system's frequency bandwidth B. When they correlated, they could be calculated using the Fourier transformation on the analogue signal $x(t)$. The result of the calculations is provided in Fig. 15. Bandwidth B = 1.27 Hz. Theoretical bandwidth $B = 1/T_i$= 1.47 Hz. A constant value N of noise spectral power density was assumed, and noise variances were determined in the system's frequency bandwidth using the following formula:

$$\sigma_i^2 = N \cdot B. \tag{5}$$

For the parameters assumed, SNR_l = 7.5 dB was obtained. The improvement in the signal-to-noise ratio was as follows when P_{no} was determined using:

- noise power $dSNR_p$= 14.3 dB,
- noise variance $dSNR_v$ = 16.0 dB,
- power of positive noise values SNR_0 = 24.1 dB.

The theoretical increase in the output signal-to-noise ratio for the correlation receipt was described using the following value:

$$dSNR_{out} = 10 \log_{10}(2B\tau), \tag{6}$$

where τ was the duration of one MLS signal cycle ($\tau = M \cdot T$).

This increase amounted to 15.8 dB and fell within the error limits equal to the increase determined on the basis of noise variances. This was confirmed by the calculations carried out for different MLS orders and different times T.

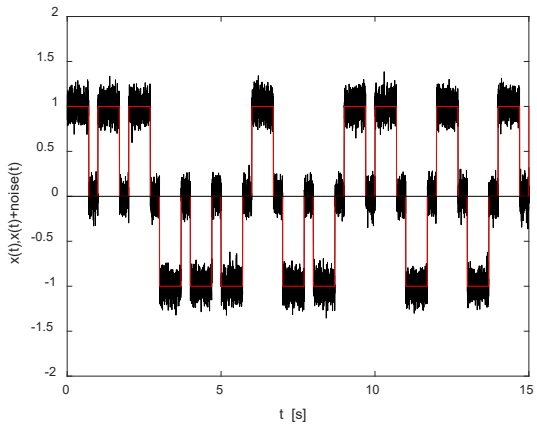

Figure 11. Analogue MLS without noise and with noise (red - without noise, black - with noise), (M = 15, T = 1 s, T_i = 0.7 s, σ = 0.1).

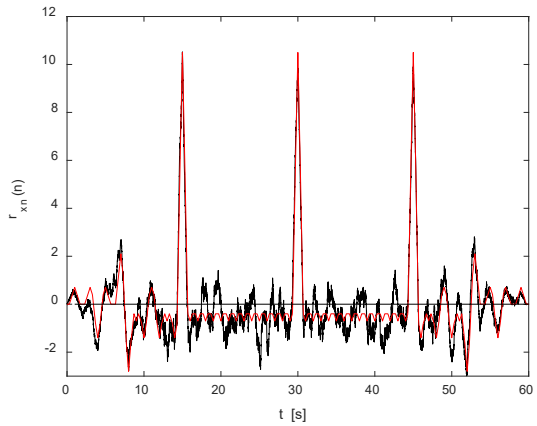

Figure 12. Functions of correlation of three analogue MLS's (red - without noise, black - with noise) (parameters as in Fig. 11, σ = 7).

4. Noise in the MLS code system

In the system under consideration, the HFM signal correlation and the analogue MLS correlation were accompanied by a convolution operation of the HFM correlation function with a rectangular pulse (see Fig. 1). It determined the current mean of the HFM correlation function, which influenced the output signal-to-noise ratio. The value of this ratio was also influenced by the parameters of the input

signal (number of elements in the sequence, bit pulse duration T, single pulse duration T_i) and target movement speed v.

The output signal-to-noise ratio (SNR_{out}) could be defined using three methods, namely relative to noise variation, noise power and power of its positive values. Figure 13 presents the absolute value of an example output signal and Fig. 14 presents its positive path. A difference in the noise level, and as a consequence different values in the output signal-to-noise ratio, could be clearly seen.

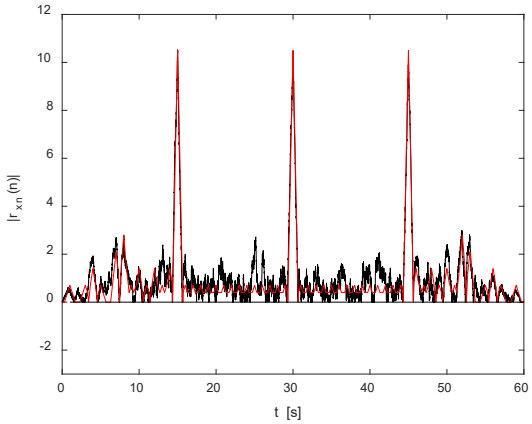

Figure 13. Absolute values of the correlation function from Fig. 12.

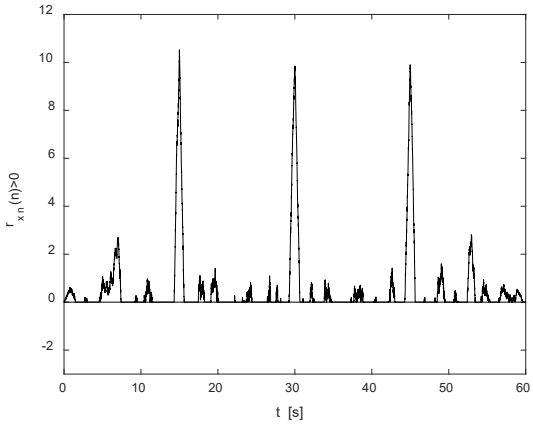

Figure 14. Positive values of the correlation function from Fig. 13.

In conventional frequency-modulated sonars this difference would be constant and determined using the formula (6). In the system under consideration with code modulation, the difference $dSNR$ was a function of input signal-to-noise ratio, as shown in Fig. 15 and Fig. 16. The curves in those and subsequent figures, were plotted for the following system parameters: (M = 15, HFM low band: f_l = 4.375 Hz; f_h = 4.875 Hz, HFM high band: f_l = 5.125, Hz, f_h = 5.625 Hz, T = 0.1 s, T_i = 0.07 s, s_o = 1).

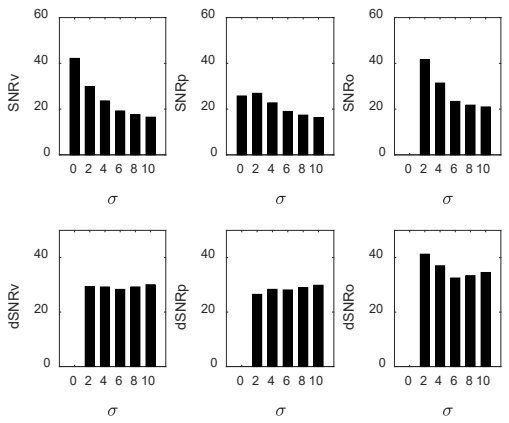

Figure 15. The output signal-to-noise ratios SNR and the difference of input and output signal-to-noise ratios $dSNR$ for v = 0 m/s

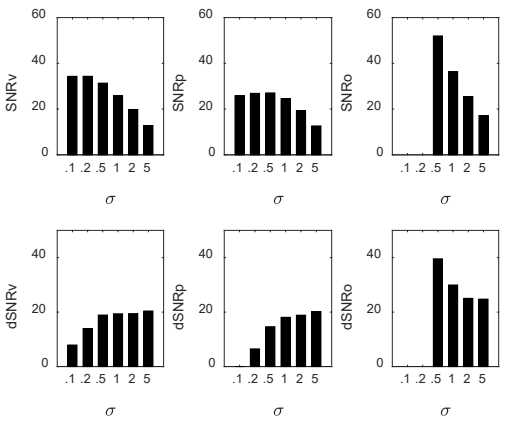

Figure 16. The output signal-to-noise ratios SNR and the difference of input and output signal-to-noise noise ratios $dSNR$ for v = 9 m/s.

In the MLS sonar under consideration constant dependence occurred for high noise (low SNR_i). For lower noise, SNR_p was almost constant as noise included side lobes of the correlation function shown in red in Fig. 12 and Fig. 13. SNR_v, systematically decreasing since it did not include constant signal component. As a result the differences $dSNR$ of signal ratios were constant. In this respect the detection properties of both sonar types could be compared. A comparable difference in signal-to-noise ratios with the conventional sonar could be determined by assuming that its bandwidth was equal to the sum of the HFM signal bandwidths and their interval, and amounted to B = (5.625 Hz - 4,375 Hz) = 1.250 Hz, with a signal duration of $\tau = M \cdot T$ = 1.5 s. According to formula (6), the value $dSNR_{out}$ = 32.7 dB, which was therefore approximately 3 dB higher than the value determined for the LFM sonar. This favourable change may be assigned to the averaging operation performed in the LFM sonar.

In both figures, when only positive noise values were observed, an increase in SNR_0 and $dSNR_0$ was visible. At higher values of SNR_i noise does not exceed the zero threshold, thus $SNR_0 = \infty$. The Doppler effect, the effects of which are illustrated in Fig. 16, worsens the detection conditions. Apart from formal improvement in the detection conditions for high noise levels, see Fig. 17. At a formally high signal-to-noise ratio, local high-value noise peaks were visible, close to the peaks of the correlation function, which significantly deteriorated the detection conditions. In classic sonars the value of detection probability and false alarm probability could be closely related to the output signal-to-noise ratio, which resulted from the Gaussian noise probability density distribution. In this sonar, the probability density distribution significantly deviated from the Gaussian distribution, see Fig. 18 and Fig. 19. With the detection threshold set to 0.3, the probability of a false alarm at v = 0 m/s amounted to PFA = 0.12, and at v = 13.5 m/s, PFA = 0.22. These values were considerably higher than the values set in the LFM sonars, where they amounted to $PFA = 10^{-4} - 10^{-6}$. This meant that a necessity to reduce the input signal-to-noise ratio in the MLS code system.

The detection conditions in the sonar were also influenced by the probability density distribution of maximum output signal amplitudes. For the example here, the sequences of maximum amplitudes $A(n)$, are shown in Fig. 20. Their corresponding charts of probability density are presented in Fig. 21 and Fig. 22.

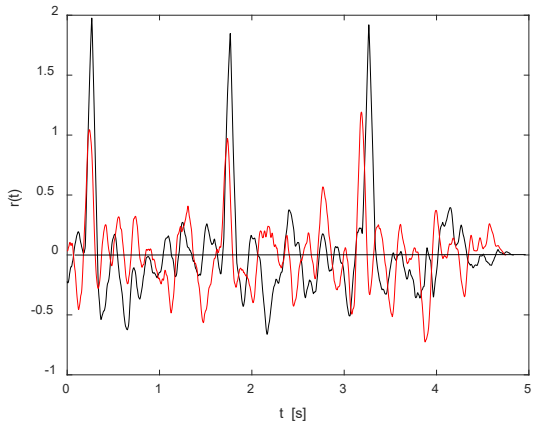

Figure 17. Output signal (black v = 0 m/s, red v =13.5 m/s, σ = 4).

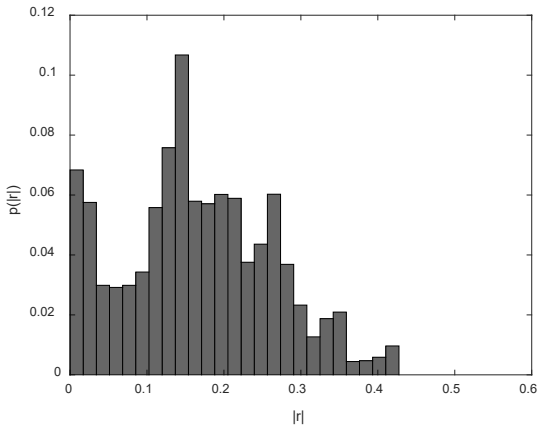

Figure 18. Probability density distribution, of output noise at v = 0 m/s.

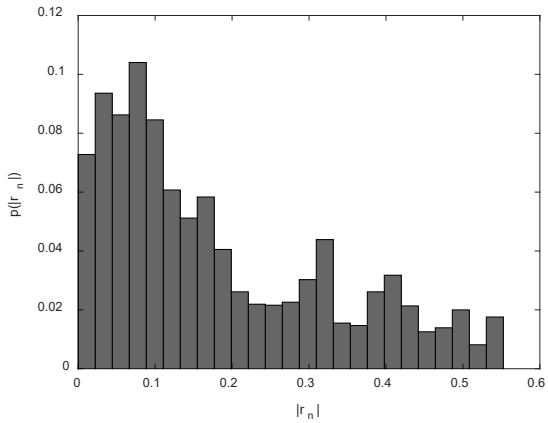

Figure 19. Probability density distribution of output noise at v = 13.5 m/s.

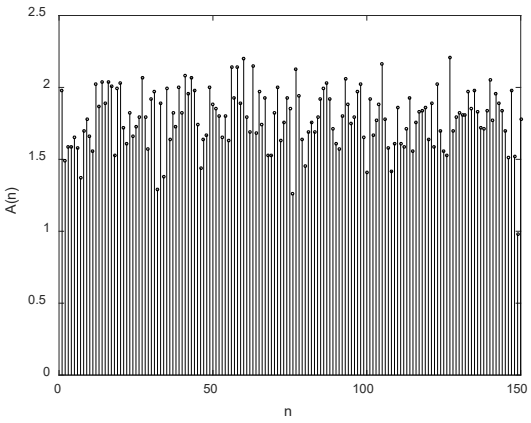

Figure 20. Sequence of maximum amplitudes of output signal at v = 0 m/s.

The probability density distribution without the Doppler effect was similar to Gaussian distribution, while higher probabilities occurred for amplitudes with higher values. With the Doppler effect, the deformation was greater. This resulted from noise with a non-zero mean value caused by the side lobes of the correlation function of the analogue MLS. At a zero target velocity the mean value of amplitudes was

$\bar{A}$ = 1.75, and standard deviation σ_A = 0.24. At v = 13.5 m/s the values were respectively $\bar{A}$ = 1.31 and σ_A = 0.28. Output signal-to-noise values determined on the basis of the above values were as follows: *SNR* = 17.2 dB and *SNR* = 13.3 dB, which were lower than the values given in Fig. 15. This means that the output signal amplitudes were not the sum of an effective signal and noise, as was the case in classic sonars. Additionally, it could be seen that if the Doppler effect occurred, the detection conditions deteriorated.

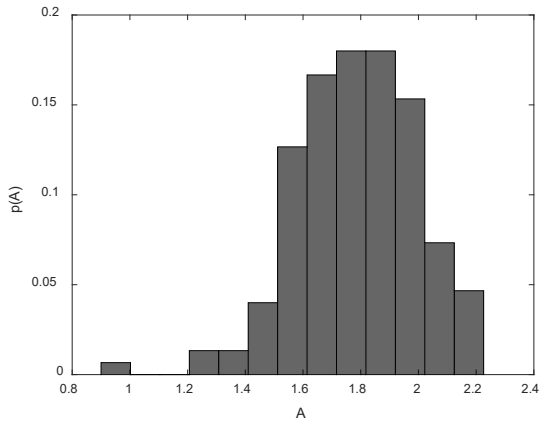

Figure 21. Probability density distribution of sequence of amplitudes from Fig. 20.

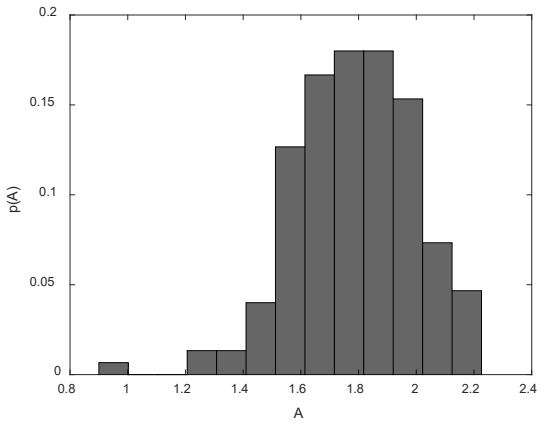

Figure 22. Probability density distribution of sequence of amplitudes for v=13.5 m/s.

The impact of the rectangle pulse length to the output signal-to-noise ratio can be illustrated at zero target velocity in Fig. 23 and at v = 9 m/s in Fig. 24. The increase in *dSNRv* was almost constant as it did not include the increase in the side lobes of the correlation function. The effect of this increase was visible for *dSNR*, where this increase decreased. According to formula (6), an increase in *dSNR* with simultaneous increase in time T_i should have been expected, which was not the case. This meant that the level of the side lobes had a greater impact on *dSNR*.

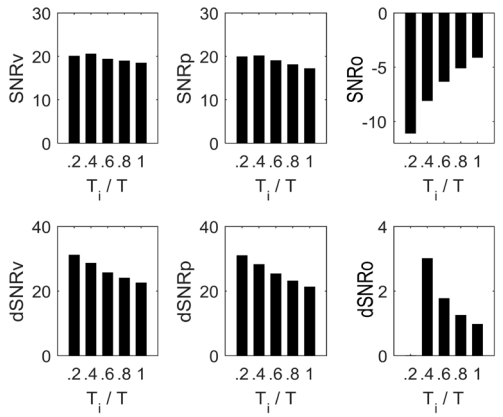

Figure 23. The output signal-to-noise ratios *SNR* and the difference of input and output signal-to-noise ratios *dSNR* as a function of pulse duration T_i (σ = 4, v = 0 m/s).

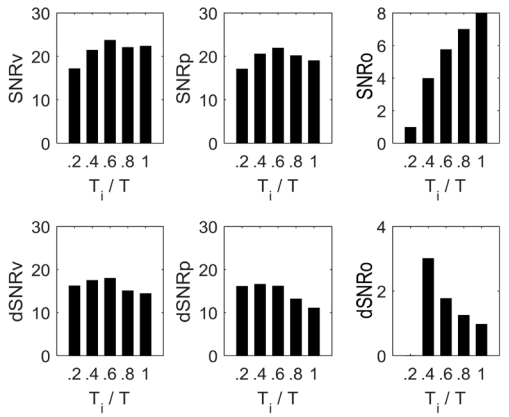

Figure 24. The output signal-to-noise ratios *SNR* and the difference of input and output signal-to-noise ratios *dSNR* as a function of pulse duration T_i (σ=1, v = 9 m/s).

The target velocity reduced the output signal-to-noise ratio and, additionally, its tendency was not constant. This was related to the time compression of a signal with the Doppler effect, as shown in Fig. 2, Fig. 4 and Fig. 5. The effect was a decrease in the peaks of the correlation function, which can be seen in Fig. 17.

The impact of the target velocity on the output signal-to-noise ratio can be seen in Fig. 25. In general, there was a tendency related to the decrease in *SNR* with the increase in velocity *v*. Visible fluctuations resulted from the variable shift in the correlation function as a function of velocity.

The effects of the increase in duration T while maintaining the MLS length (increasing the system's range) can be seen in Fig. 26. At greater durations, T, the ratio SNR for zero target velocity was almost constant. A non-zero target velocity caused a decrease in the output signal-to-noise ratio and additionally led to its fluctuations. This was an effect of the aforementioned shifts in the correlation functions over time.

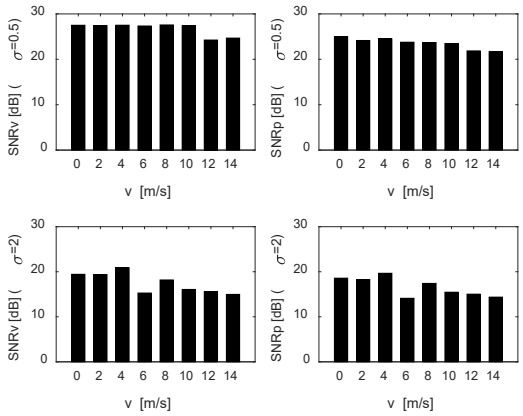

Figure 25. Impact of the target velocity on the output signal-to-noise ratio.

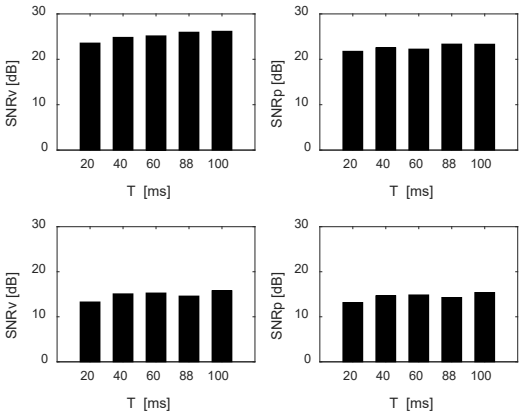

Figure 26. Impact of the bit duration T on the output signal-to-noise ratio (upper pictures - v = 0 m/s, lower - v = 6 m/s).

Fig. 27 and Fig. 28 illustrate the impact of the order M of the MLS (the number of elements in the sequence $N = M^2 - 1$) on the output signal-to-noise ratio. At zero velocity an increase in SNR and $dSNR$ occurred. This was caused by a proportional increase in the MLS code correlation function relative to the number of its elements. At non-zero target velocity, fluctuations in SNR and $dSNR$ were visible, their cause being described above.

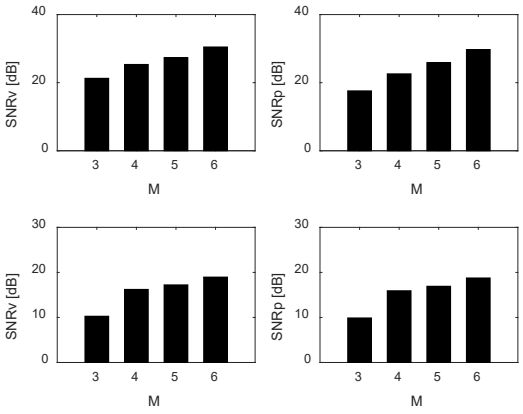

Figure 27. Influence of M model order of the MLS code on the output signal-to-noise ratio: (upper picture v=0 m/s, lower v =6 m/s), (T = 40 ms, T_i = 28 ms, SNR_i = 0.38 dB).

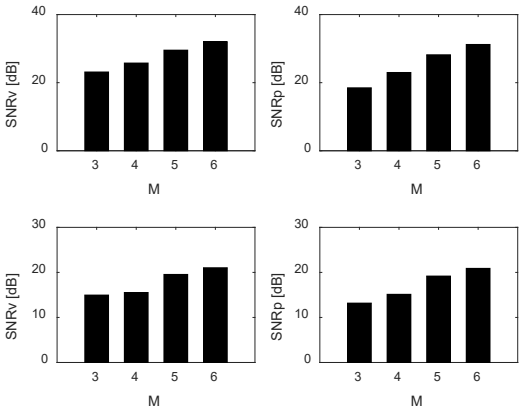

Figure 28. Influence of M model order of the MLS code on the output signal-to-noise ratio (upper pictures v=0 m/s, lower v =6 m/s), (T = 100 ms, T_i = 70 ms, SNR_i = 0.38 dB).

5. Conclusions

Previous publications demonstrated that the application of MLS code modulation in the silent sonar resulted in a considerable reduction in target measurement error relative to conventional sonars with linear or hyperbolic frequency modulation [7, 8]. During the engineering design stage of the sonar with MLS modulation, the signal parameters can be optimised (order of MLS model, duration T and duration T_i) for measurement error reduction and measurement resolution. It is also necessary to optimise in terms of the detection conditions depending on the output signal-to-noise ratio relative to the input signal-to-noise ratio. The simulation results presented above form the basis for this type of optimisation. Moreover the simulation results allow two general conclusions to be drawn, namely that the detection conditions in the

sonar with MLS modulation are similar to the conditions prevailing at zero target velocity in a comparable LFM or HFM sonar, and that at higher target velocities the conditions in the MLS sonar slightly deteriorate.

The significant issue of the impact of noise on the target distance measurement error, which was not discussed in this study as it exceeded the framework of this publication, will be the subject matter of the next publication.

Additional information

The authors declare: no competing financial interests and that all material taken from other sources (including their own published works) is clearly cited and that appropriate permits are obtained.

References

1. H. DeFerrari, J. Wylie; Ideal signals and processing for continuous active sonar; Acoustical Society of America, Proceedings of Meetings on Acoustics (ICA 2013 Montreal Canada), 19, 055058, 2013
2. S. J. Lourey; Frequency Hopping Waveforms for Continuous Active Sonar; Proceedings of 2015 IEEE International Conference on Acoustics, Speech, and Signal Processing, 1832 – 1835, Brisbane 2015
3. R. Van Vossen, S. P. Beerens, E. Vander Spek; Anti-Submarine Warfare with Continuously Active Sonar; Sea Technology, 2011, 52(11), 33-35
4. J. Marszal, R. Salamon; Silent Sonar for Maritime Security Applications; Acoustical Society of America, Proceedings of Meetings on Acoustics (ECUA 2012 Edinburgh UK), 17, 070082, 2013
5. J. Marszal, R. Salamon; Distance Measurement Errors in Silent FM-CW Sonar with Matched Filtering; Metrology and Measurement Systems, 2012, 19 (2), 321-332
6. J. Marszal; Experimental Investigation of Silent Sonar; Archives of Acoustics, 2014, 39(1), 103-115
7. A. Jedel, J. Marszal, R. Salamon; Continuous wave sonar with hyperbolic frequency modulation keyed by pseudo-random sequence; Hydroacoustics, 2016, 19, 185-196
8. A. Jedel, J. Marszal, R. Salamon; Analysis of distance measurement errors in CW FM sonar with MLS code modulation; Hydroacoustics, 2017, 20, 75-84
9. I. Kochańska, R. Salamon, J. Schmidt, A. Schmidt; Study of the Performance of DSSS UAC System Depending on the System Bandwidth and the Spreading Sequence;Sensors, 2021, 21(7), 2484
10. I. Kochańska; A New Direct-Sequence Spread Spectrum Signal Detection Method for Underwater Acoustic Communications in Shallow-Water Channel; Vibrations in Physical Systems, 2021, 32(1), 2021106
11. J. H. Schmidt; Using Fast Frequency Hopping Technique to Improve Reliability of Underwater Communication System; Applied Sciences, 2020, 10(3), 1172
12. N. Levanon, E. Mozeson; Radar Signals, John Wiley & Sons, 2004